Proceedings of the 2005 IEEE/ASME
International Conference on Advanced Intelligent Mechatronics
Monterey, California, USA, 24-28 July, 2005

Torque Model for Design and Control of a Spherical Wheel Motor

Kok-Meng Lee* and Hungsun Son

Abstract— This paper presents a method of deriving the torque model for a three degrees of freedom (3-DOF) spherical motor such as a variable-reluctance spherical motor (VRSM) or a spherical wheel motor (SWM). The SWM (much like the VRSM capable of offering three-DOF in a single joint) offers the ability to spin continuously while the rotor shaft can be tilted arbitrarily. We derive a closed-form torque model and demonstrate its use for designing the switching controller based the principle of push-pull operation for the SWM. The closed-form torque model given here greatly reduces the torque computation, and simplifies the design of the switching controller.

Keywords- *actuators, torque model, stepper control*

I. Introduction

Mobile vehicles (such as car wheels [1] [2], propellers for boats, helicopter or underwater vehicle), gyroscopes, and machine tools require orientation control of a rotating shaft. The growing interests in fuel-cell technology and low-cost electric vehicles have motivated a number of researchers to develop alternative design of in-wheel motors. Existing designs are typically single-axis devices; orientation control of the rotating shafts must be manipulated by an external mechanism. These multi-axe spinners are generally bulky, slow in dynamic response, and lack of dexterity in negotiating the orientation of the rotating shaft.

An alternative to these multi-axis spinners is a spherical motor that takes a number of forms including the stepper [3], induction motor [4] [5], direct-current motor [6] [7] [8], variable-reluctance motor [9] [10] [11], ultrasonic motor [12] and also in [13]. Compared with its counterparts, the spherical stepper has a relatively large range of motion, simple, compact in design, and possesses isotropic properties in motion. In addition, it can operate in open-loop and thus provides an incentive for further development as a SWM.

The basic concept of a spherical stepper was originally proposed by [3]. The dynamic model of a particular VRSM can be found in [9], where the torque model is a quadratic function of the current inputs to the stator coils. Reference [10] studied the method to place the rotor poles for stepping motion on a structure similar to that suggested in [3]. A similar study can also be found in [11], in which they derived the torque vector and the back electromotive forces in closed form based on an analytical magnetic field distribution. Most of the spherical motor research has focused on developing alternative design concepts and non-contact sensors for measuring three-DOF orientation for feedback control. More recently, the interest to derive a closed-form solution to the inverse torque model has led [14] to design a VRSM that has a linear torque-current relationship. The torque model involves a large number of individual torque component terms, each of which requires the computation of a time-vary vector cross-product in 3D space. For real-time control particularly involving orientation feedback, this represents a significant computational burden. These existing spherical motors (motivated by the advance in robotic technology) have pre-dominantly been designed for wrist like motions; the primary interest has been the control of three-DOF orientation displacements.

Motivated by the growing interests in high performance in-wheel motors for electric vehicles, we explore in [15] the feasibility of designing a VRSM that offers orientation control of the rotating shaft, which led to the design concept of a SWM. This paper focuses the following:

1. We present the method of deriving a closed-form torque model for a SWM, which greatly reduces the computation and simplifies the controller design. We start with an approximate model that consists of two electromagnets (EM) and a permanent magnet (PM) in 3D space, and then extends it to a more general configuration using multiple sets of 2EM-1PM models.
2. We describe the method of controlling the rotor orientation while allowing it to spin continuously using the principle of push-pull operation in open-loop. Specifically, we provide a method for deriving different switching sequences for open-loop speed control.
3. We illustrate the switching controller design for a SWM that has 8 rotor PM pole-pairs and 10 stator EM pole-pairs. As will be shown, this switching controller essentially functions as an electronic gear transmission for the SWM.

II. Torque Formulation for SWM Design

Reference [14] derived a general torque model for a VRSM based the principle of variable-reluctance. We consider here a design where the rotor poles of the VRSM are permanent magnets (PM's) and the stator electromagnets (EM's) are coils wound on non-ferromagnetic cores. The i^{th} component torque acting on the rotor can be approximated as a linear combination of stator currents:

$$T_i \approx \mathbf{u}_r^{\mathrm{T}} \frac{\partial [L_{rs}]}{\partial \theta_i} \mathbf{u}_s = [K(\mathbf{q})] \mathbf{u}_r^{\mathrm{T}} \mathbf{u}_s \qquad (1)$$

Manuscript received March 15, 2005. This work was supported in part by the Georgia Agricultural Technology Research Program (ATRP) and the U.S. Poultry and Eggs (USPE) Association.

*Corresponding author-K.-M. Lee, Professor, Woodruff School of Mechanical Engineering, Georgia Institute of Technology, Atlanta, Georgia 30332-0405, USA (e-mail: kokmeng.lee@me.gatech.edu)

H. Son, Ph.D. Candidate, Woodruff School of Mech. Eng, Georgia Tech, Atlanta, Georgia 30332, USA (e-mail: gtg208j@mail.gatech.edu)

where $\mathbf{q} = [\phi \quad \alpha \quad \beta]^{\mathrm{T}}$ is an orientation vector in spherical coordinates with angles defined in Fig. 1; and the subscripts "*r*" and "*s*" denotes the rotor and stator respectively.

Unlike the VRSM where the PM's and EM's are placed on the vertices of regular polygons, equally-spaced magnetic poles are layered on circular planes for a SWM as illustrated in Fig. 1(b), where *R* is the radius of the spherical rotor; γ is the angle between the circular plane from the *XY* plane; and δ is the angle between the two adjacent poles (PM's or EM's) on the circumference. The spherical stator and rotor are concentric, and the air-gap between them is very small as compared to the radius *R*. The magnetization axis of the stator EM is defined mathematically by the position vector:

$$\mathbf{s}_j = R\left[\cos\gamma_s \cos(j-1)\delta_s \quad \cos\gamma_s \sin(j-1)\delta_s \quad \sin\gamma_s\right]^{\mathrm{T}} \tag{2}$$

where $j = 1, 2, \ldots, m_s$; and γ_s is the angle between the plane of stator poles and the XY plane as shown in Fig.2. Similarly, the magnetization axis of the rotor PM is given in the stator frame XYZ by (3):

$$\mathbf{r}_k = R[\boldsymbol{\Gamma}]\left[\cos\gamma_r \cos(k-1)\delta_r \quad \cos\gamma_r \sin(k-1)\delta_r \quad \sin\gamma_r\right]^{\mathrm{T}} \tag{3}$$

where $k = 1, 2, \ldots, m_r$. The coordinate transformation matrix $[\boldsymbol{\Gamma}]$ from the rotor to the stator frames is given by

$$[\boldsymbol{\Gamma}] = \begin{bmatrix} C_\phi C_\alpha C_\beta - S_\phi S_\beta & C_\phi C_\alpha S_\beta + S_\phi C_\beta & -C_\phi S_\alpha \\ S_\phi C_\alpha C_\beta - C_\phi S_\beta & S_\phi C_\alpha S_\beta + C_\phi C_\beta & -S_\phi S_\alpha \\ S_\alpha C_\beta & S_\alpha S_\beta & C_\alpha \end{bmatrix} \tag{4}$$

where the cosine and sine of ϕ is denoted by C_ϕ and S_ϕ.

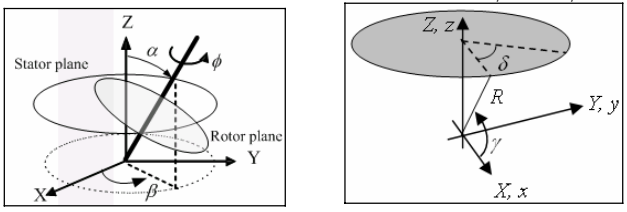

(a) Spherical ordinates (b) Plane of pole location

Fig. 1 Parameters defining coordinate system and pole layout

As the magnetic circuit is linear, the torque generated from the changes of flux linkages can be written in XYZ frame as

$$\mathbf{T} = [T_X \quad T_Y \quad T_Z]^{\mathrm{T}} = \sum_{k=1}^{m_r} \mathbf{T}_{rk} = \sum_{k=1}^{m_r}\sum_{j=1}^{m_s} \mathbf{T}_{jk} \tag{5}$$

$$\mathbf{T}_{jk} = \begin{cases} 0 & \text{if } |\mathbf{s}_j \times \mathbf{r}_k| = 0 \\ u_{rk} u_{sj} f(\varphi_{jk})(\mathbf{s}_j \times \mathbf{r}_k)/|\mathbf{s}_j \times \mathbf{r}_k| & \text{if } |\mathbf{s}_j \times \mathbf{r}_k| > 0 \end{cases}$$

$$\varphi_{jk} = \left|\cos^{-1}\left(\frac{\mathbf{s}_j^{\mathrm{T}}\mathbf{r}_k}{|\mathbf{s}_j||\mathbf{r}_k|}\right)\right| \tag{6}$$

where $\mathbf{T}_{rk}$ is the torque as a result of the interaction between the k^{th} PM with m_s EM's; u_{rk} defines the polarity of the k^{th} PM; u_{sj} is dimensionless current flowing through the j^{th} EM; and $f(\varphi_{jk})$ is a torque function that can be derived from the computed data using the finite-element (FE) analysis [14] or obtained experimentally [9].

The SWM offers the ability to spin continuously (much like a brushless DC motor) about the rotor z-axis while the shaft can be tilted arbitrarily from its Z-axis:

$$\hat{\mathbf{z}} = \left[S_\alpha C_\beta \quad S_\alpha S_\beta \quad C_\alpha\right]^{\mathrm{T}} \tag{7}$$

The torque component about the z-axis is given by

$$T_z = T_X S_\alpha C_\beta + T_Y S_\alpha S_\beta + T_Z C_\alpha \tag{8}$$

Since $\boldsymbol{s}_j$ and $\boldsymbol{r}_k$ are positive vectors, the torque direction of each term on the right-hand-side of (5) depends on u_{rk} and u_{sj}. Computation of the resultant torque involves summing $m_s \times m_r$ terms of $\mathbf{T}_{jk}$ each of which includes a unit cross-product $(\mathbf{s}_j \times \mathbf{r}_k / |\mathbf{s}_j \times \mathbf{r}_k|)$. Since the rotor and stator poles are symmetrically arranged and the torque function $f(\varphi_{jk})$ generally has a limited range, the torque model (5) can be reduced to deriving a few non-zero $\mathbf{T}_{jk}$. For this, we consider a 2EM-1PM model and then extend to a general case by constructing multiple sets of 2EM-1PM models.

A. 2EM-1PM model

Without loss of generality, we set

$$-u_{r(k+1)} = u_{rk} = 1, \text{ where } u_{r1} = -1 \tag{9}$$

and

$$f(\varphi_{jk}) = 0 \quad |\varphi_{jk}| > \delta_s \tag{10}$$

Equation (10) can be justified with the illustration as shown in Fig. 2. If the torque function has a range larger than δ_s, there will be conflicting torques acting on the same rotor PM.

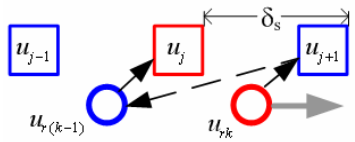

Figure 2 Conflicting torques on the rotor pole-pair

For the 2EM-1PM model shown in Fig. 3, Equation (5) can be reduced to (11):

$$\mathbf{T}_{\Delta k} = (-1)^k \left[f(\varphi_{jk}) \frac{\mathbf{s}_j \times \mathbf{r}_k}{\|\mathbf{s}_j \times \mathbf{r}_k\|} u_{sj} + f(\varphi_{(j+1)k}) \frac{\mathbf{s}_{j+1} \times \mathbf{r}_k}{\|\mathbf{s}_{j+1} \times \mathbf{r}_k\|} u_{s(j+1)} \right] \tag{11}$$

where the index *j* is chosen such that

$$\varphi_{jk}, \varphi_{j(k+1)} \le \delta_s \tag{11a}$$

Equations (9) and (10) reduce the number of $\mathbf{T}_{jk}$ terms from $m_s \times m_r$ to $2m_r$ where $m_s > m_r$. To facilitate our discussions, we define in Fig. 3(a) the following parameters:

Angle between $\mathbf{r}_k$ and XY plane:

$$\alpha_k = \tan^{-1}\left(r_{k3} / \sqrt{r_{k1}^{\,2} + r_{k2}^{\,2}}\right) \tag{12a}$$

where $\mathbf{r}_k = [r_{k1} \quad r_{k2} \quad r_{k3}]^{\mathrm{T}}$.

Perpendicular distance from k^{th} PM to the chord *c*, between j^{th} and $(j+1)^{th}$ EM's:

$$h_k = 2R \sin\left(\frac{\gamma_s - \alpha_k}{2}\right) \tag{12b}$$

Angle between the projection of $\mathbf{r}_k$ on *XY* plane from the *X*-axis at initialization (i.e. *XYZ* and *xyz* frames coincide):

$$\phi_k = \phi + (k-1)(\delta_r - \delta_s) \tag{12c}$$

When $\alpha = 0°, \phi_k = \phi$. The index *j* in (11) for the EM with respect to the k^{th} PM can be found from (12d):

$$j = \text{int}\left(\phi_k / \delta_s\right) + k \tag{12d}$$

where int(•) denotes the integer of its argument.

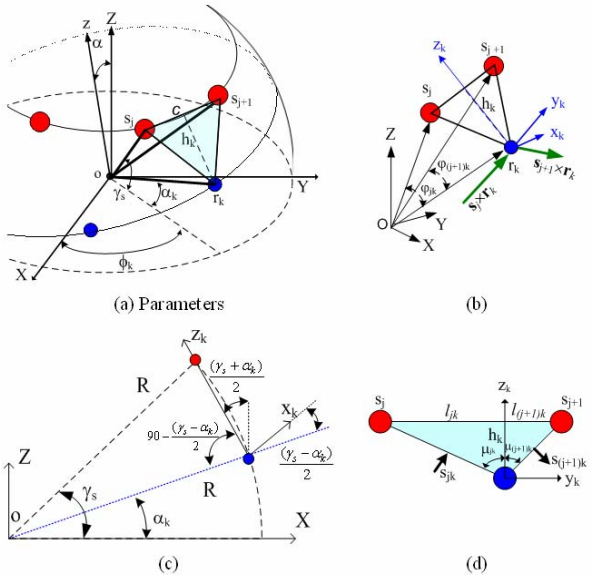

Fig.3 Triangle of PM and EM's on the projected plane corresponding axes

B. Finding the cross-product term

To derive the unit cross product ($\mathbf{s}_j \times \mathbf{r}_k / |\mathbf{s}_j \times \mathbf{r}_k|$) in the torque model, we define a local coordinate frame ($x_k y_k z_k$) at the k^{th} PM as shown in Fig. 3(d). The k^{th} PM and its two adjacent EM's, j^{th} and $(j+1)^{\text{th}}$, form a triangular plane (Fig. 3a). The x_k axis is normal to the triangular plane and the z_k axis lies on the triangular plane pointing towards and perpendicular to the chord c (between the two EM's) as detailed in Fig. 3(b). The transformation from $x_k y_k z_k$ to XYZ is given by (13)

$$\begin{bmatrix} \hat{x}_k \\ \hat{y}_k \\ \hat{z}_k \end{bmatrix} = \begin{bmatrix} C_{(\gamma_s+\alpha_k)/2} C_{\phi_k} & C_{(\gamma_s+\alpha_k)/2} S_{\phi_k} & S_{(\gamma_s+\alpha_k)/2} \\ -S_{\phi_k} & C_{\phi_{rk}} & 0 \\ -S_{(\gamma_s+\alpha_k)/2} C_{\phi_k} & -S_{(\gamma_s+\alpha_k)/2} S_{\phi_k} & S_{(\gamma_s+\alpha_k)/2} \end{bmatrix} \begin{bmatrix} \hat{X} \\ \hat{Y} \\ \hat{Z} \end{bmatrix} \tag{13}$$

We resolve the cross-product ($\mathbf{s}_j \times \mathbf{r}_k$) into two components: The component normal to the plane as shown in Fig. 3(c) lies mainly along the radial axis of the rotor pole, which generates no torque. Only a small fraction of this normal component contributes to the torque in (11) and is neglected to trade-off for a closed-form torque model for designing the switching controller. The 2nd component accounts for the torque on the $y_k z_k$ plane denoted here as $\mathbf{s}_{jk} \approx \mathbf{s}_j \times \mathbf{r}_k$, or $\mathbf{s}_{jk} \bullet (-l_{jk} \hat{y}_k \times h_k \hat{z}_k) = 0$

From Fig. 3(c), we have $\mathbf{s}_{jk} = h_k \hat{y}_k + l_{jk} \hat{z}$

or
$$\mathbf{s}_{jk} / \|\mathbf{s}_{jk}\| = (h_k \hat{y}_k + l_{jk} \hat{z}_k) / \sqrt{h_k^2 + l_{jk}^2} \tag{14}$$

$$\frac{\mathbf{s}_j \times \mathbf{r}_k}{\|\mathbf{s}_j \times \mathbf{r}_k\|} \approx \begin{bmatrix} -C_{\mu_{jk}} S_{\phi_k} - S_{\mu_{jk}} S_{(\gamma_s+\alpha_k)/2} C_{\phi_k} \\ C_{\mu_{jk}} C_{\phi_k} - S_{\mu_{jk}} S_{(\gamma_s+\alpha_k)/2} S_{\phi_k} \\ S_{\mu_{jk}} \end{bmatrix}^T \begin{bmatrix} \hat{X} \\ \hat{Y} \\ \hat{Z} \end{bmatrix} \tag{14a}$$

Similarly,

$$\frac{\mathbf{s}_{j+1} \times \mathbf{r}_k}{\|\mathbf{s}_{j+1} \times \mathbf{r}_k\|} \approx \begin{bmatrix} -C_{\mu_{(j+1)k}} S_{\phi_k} + S_{\mu_{(j+1)k}} S_{\tilde{\alpha}_k} C_{\phi_k} \\ C_{\mu_{(j+1)k}} C_{\phi_k} + S_{\mu_{(j+1)k}} S_{\tilde{\alpha}_k} S_{\phi_k} \\ -S_{\mu_{jk}} \end{bmatrix}^T \begin{bmatrix} \hat{X} \\ \hat{Y} \\ \hat{Z} \end{bmatrix} \tag{14b}$$

where
$$l_{jk} = \sqrt{(2R\sin(\varphi_{jk}/2))^2 - h_k^2} \; ; \; l_{(j+1)k} = c - l_{jk}$$

$$C_{\mu_{jk}} = \cos\mu_{jk} = h_k / \sqrt{h_k^2 + l_{jk}^2} \; ; S_{\mu_{jk}} = \sin\mu_{jk} = l_{jk} / \sqrt{h_k^2 + l_{jk}^2}$$
$$C_{\mu_{(j+1)k}} = \cos\mu_{(j+1)k} \; \text{; and} \; S_{\mu_{(j+1)k}} = \sin\mu_{(j+1)k}$$

C. Torque Model in Closed Form

The torque $\mathbf{T}_{rk}$ for the 2EM-1PM model is given by

$$\mathbf{T}_{\Delta k} = (-1)^k \left\{ {}^1\mathbf{T}_{\Delta k} + {}^2\mathbf{T}_{\Delta k} \sin\left[(\gamma_s + \alpha_k)/2\right] \right\} \begin{bmatrix} u_{sj} \\ u_{s(j+1)} \end{bmatrix} \tag{15}$$

where
$${}^1\mathbf{T}_{\Delta k} = \begin{bmatrix} -f(\varphi_{jk}) C_{\mu_{jk}} S_{\phi_k} & -f(\varphi_{j+1,k}) C_{\mu_{j+1,k}} S_{\phi_k} \\ f(\varphi_{jk}) C_{\mu_{jk}} C_{\phi_k} & f(\varphi_{j+1,k}) C_{\mu_{j+1,k}} C_{\phi_k} \\ f(\varphi_{jk}) S_{\mu_{jk}} & -f(\varphi_{j+1,k}) S_{\mu_{j+1,k}} \end{bmatrix} \tag{15a}$$

$${}^2\mathbf{T}_{\Delta k} = \begin{bmatrix} -f(\varphi_{jk}) S_{\mu_{jk}} C_{\phi_k} & f(\varphi_{j+1,k}) S_{\mu_{(j+1)k}} C_{\phi_k} \\ -f(\varphi_{jk}) S_{\mu_{jk}} S_{\phi_k} & f(\varphi_{j+1,k}) S_{\mu_{(j+1)k}} S_{\phi_k} \\ 0 & 0 \end{bmatrix} \tag{15b}$$

In summary, the torque generated by the 2EM-1PM model for a specified rotor orientation can be computed as follows: First, compute $\mathbf{r}_k$ using (3) and α_k and h_k from (12). Next, calculate φ_{jk} using (6). Then, obtain the cross-product using (14). Finally, calculate the torque using (15).

We extend the 2EM-1PM model to a more configuration for computing the resultant torque. First, consider the left-hand-side in Fig. 4, where a rotor PM u_{rk} (blue open circle) interacts with four EM's. In Fig. 4 where the subscript "s" is dropped for simplicity, $\bar{u}_{sj}$ and u_{sj} are a conjugate pair, which have the same X and Y coordinates but their Z-ordinates are equal in magnitude but opposite in sign. Similarly, $\bar{u}_{s(j+1)}$ and $u_{s(j+1)}$ are conjugate pairs. Using two separate 2EM-1PM models given by (15), the net torque for this 4EM-1PM model can be written as

$$\mathbf{T}_{rk} = \mathbf{T}_{\Delta k} + \bar{\mathbf{T}}_{\Delta k} \tag{16}$$

where $\mathbf{T}_{\Delta k}$ and $\bar{\mathbf{T}}_{\Delta k}$ result from the interaction between u_{rk} and (u_{sj}, $u_{s(j+1)}$) and between u_{rk} and ($\bar{u}_{sj}$, $\bar{u}_{s(j+1)}$) respectively.

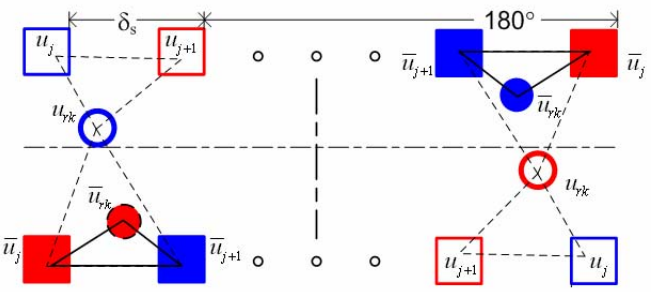

Fig. 4 Extension of 2EM-IPM to general cases

Next, we consider a symmetrical structure by adding four identical stator poles 180° out-of-phase (right-hand-side of Fig. 4) such that the eight stator poles form four pairs of EM's with their magnetization axes passing through the stator center. The net torque for this 8EM-2PM model is simply twice that of the two 4EM-1PM models given by (16).

Finally, we consider a 3rd configuration where two additional PM's (red solid circles) are added to the structure discussed earlier. In Fig. 4, $\overline{u}_{rk}$ is the conjugate of u_{rk} in the rotor xyz coordinates. The net torque can be computed using two 4EM-2PM models, one with u_{rk} and the other with $\overline{u}_{rk}$.

III. Design and Operational Principle

As will be shown, the torque computation and the switching controller design can be further reduced by exploiting by the pole layout of the VRSM.

A. Rotor and Stator Pole Layout

Figs. 5(a) - 5(c) show three symmetrical configurations of rotor PM's on circular planes: Fig. 5(a) shows a typical rotor PM pole-pair (PMpp); the polarities of the PM's of a PMpp depend on whether the number of PMpp's on the plane is odd or even. When the number of the PMpp's is odd, the polarities of each PMpp are opposite, Fig. 5(a). On the other hand, the polarities are the same when the number of PMpp's is even, Fig. 5(b). Fig. 5(c) shows two layers of PMpp's, each of which has four PM's. All the four PMpp's point radially towards the rotor center but unlike those in the single layer, the planes formed by the PMpp's are perpendicular to the XY plane and the polarities of each PMpp are opposite.

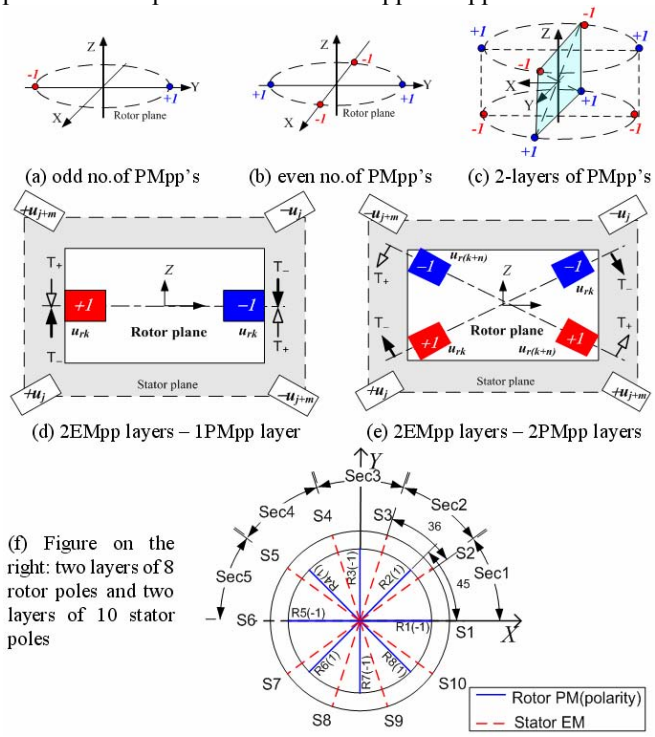

Fig. 5: Types of design configurations; (a) odd number of rotor PM pole-pair, (b) even number of rotor PM pole-pairs, (c) double-layer of rotor PM pole-pairs, (d) double-layer-stator/single-layer-rotor with odd pole-pairs, (e) double-layer-stator/double-layer-rotor (even pole-pairs), (f) plan view showing the initial locations of 8 PM's and 10 EM's.

There are two layers of stator EM pole-pairs (EMpp's) in VRSM as illustrated in Figs. 5(d) and 5(e). The EMpp's are arranged in pairs on a plane perpendicular to the *XY* plane and point radially towards the stator center. The EM polarities can be externally controlled. Due to the page limit, we denote the number of PMpp's and EMpp's as m_r and m_s and discuss only even number of PMpp's and EMpp's from here on. Clearly, a SWM with odd number of PMpp's and EMpp's can be designed following the same procedure.

B. Push-pull Interaction between Stator and Rotor Poles

The VRSM operates in two different modes; static rotor orientation control, and continuous spin as a SWM.

The rotor orientation is regulated on the principle of push-pull operation. As illustrated in Figs. 5(d) and 5(e), the inclination from the *Z*-axis is manipulated using two opposing torques, T_+ and T_-, about the axis normal to the plane that contains the current inputs u_{sj} and $u_{s(j+m)}$ producing the torques. The specific polarities of the EMpp's depend on the PMpp layout; for example, $u_{s(j+m)} = -u_{sj}$ in Fig. 5(d) while in Fig. 5(e), $u_{s(j+m)} = u_{sj}$ to maintain the rotor at zero inclination. In either case, any perturbation will result in a differential torque $\Delta\mathbf{T}$ driving the rotor to its equilibrium. For this push-pull operation, the torque model is written in the following form:

$$T_i = T_{i+} + T_{i-} + \Delta T_i \tag{17}$$

$$T_{i+} = \left(T_i \pm \Delta T_i\right)/2 \text{ and } T_{i-} = \left(T_i \mp \Delta T_i\right)/2 \tag{18}$$

where the subscript "*i*" denotes the torque components in the *X, Y* and Z directions; $T_{i\pm}$ are the static torques; and ΔT_k is the dynamic torque. The differential torque ΔT_k represents the 'driving torque' because it causes the rotor to move. However, to maintain the rotor shaft at a particular inclination (α,β), a 'holding torque' $T_{i\pm}$ must be applied.

The basic modes are as follows:

1) To regulate the rotor at a desired steady-state orientation, the torque must satisfy the following:

$$\mathbf{T} + \mathbf{T}_{\mathrm{L}} = 0 \text{ where } \Delta\mathbf{T} = 0 \text{ and } \left\|\mathbf{T}_+\right\| = -\left\|\mathbf{T}_-\right\| \neq 0 \tag{19}$$

where $\mathbf{T}_{\mathrm{L}}$ accounts for external load. A change in rotor position from any equilibrium requires a differential current to be applied to generate the required $\Delta\mathbf{T}$.

2) To spin about the rotor axis at a constant rate while regulate the rotor at the desired inclination, a driving torque ΔT_z must be maintained in addition to the application of the extraneous torque $T_{i\pm}$.

Since T_X, T_Y, and T_Z are orthogonal and linear functions of the currents, we decompose u_{sj} into three independent components:

$$u_{sj} = u_{\phi j}\left(1 + u_{\alpha j} + u_{\beta j}\right) \quad j=1,2,\ldots m_s \tag{20}$$

where $u_{\phi j}$ governs the spin motion via T_Z; and $u_{\alpha j}$ and $u_{\beta j}$ are the incremental factors regulating the rotor inclination about the *Y*- and *X*-axes through T_Y and T_X respectively. To spin an inclined rotor at a constant rate, the input $u_{\phi j}$ must not contribute to T_Y and T_X.

C. Design Parameters

To facilitate the discussions on the design of a switching controller, we define two design parameters; plane angle of symmetry, and minimum phase angle:

Plane angle of symmetry

$$\psi_{sym} = LCM(\delta_r, \delta_s) \le 180° \tag{21}$$

where ψ_{sym} in degrees; and LCM is the least common multiplier of its arguments. There are n_{sym} symmetric regions:

$$n_{sym} = \text{int}\left(360°/\psi_{sym}\right) \tag{22}$$

For example, the design (m_s =12 and m_r =18) has three symmetric regions (ψ_{sym}=60°) and that (m_s =10 and m_r =8) has two (ψ_{sym}=180°).

Minimum Phase angle

$$\psi_{\min} = GCD(\delta_r, \delta_s) \tag{23}$$

where GCD is the greatest common divisor of its arguments. The number of drive modes is equal to

$$n_{\max} = \text{int}\left(\delta_r/\psi_{\min}\right) \tag{24}$$

Different switching sequences for the Z-axis rotation can be designed based on n number of ψ_{min} or

$$\phi = \varphi_{11} = n\psi_{\min} \text{ where } n \le n_{\max}$$

Each n corresponds to a quasi-static location, at which at least one pair of PM and EM on the XY-plane are aligned. The resolution of the spin motion depends on the drive mode for a given design configuration. As will be demonstrated in Section IV.C, the design parameters can be useful when designing an electronic gear for the SWM.

D. Starting Torque

In order to have a high starting torque to overcome the rotor inertia when the SWM accelerates from rest, we derive the starting torque for a class of designs where $m_s > m_r$, $\delta_s < \delta_r < 2\delta_s$. From (12c) and (12d), $j = k$ for $\psi_{\min} = \delta_r - \delta_s$ and $k \le n_{\max}$ .The Z component torque has the following form:

$$\frac{T_Z}{n_{sym}} = -c_{1Z}u_{s1} + \sum_{j=2}^{m_s/n_{sym}} (-1)^j c_{jZ}u_{sj} - c_{(m_s/n_{sym})Z}u_{s(1+m_s/n_{sym})} \tag{25}$$

where $c_{1Z}(\varphi_{11}) = f\left(\varphi_{11}\right)\sin\mu_{11}$; $c_{(m_s/n_{sym})Z}(\varphi_f) = f\left(\varphi_f\right)\sin\mu_f$

$$c_{jZ}\left(\varphi_{j-1,j-1}, \varphi_{jj}\right) = f\left(\varphi_{j-1,j-1}\right)\sin\mu_{j-1,j-1} + f\left(\varphi_{jj}\right)\sin\mu_{jj};$$

and the subscript $f = \left(m_s/n_{sym}\right)\left(m_s/n_{sym}\right)$. From the XY projection, $\varphi_{j+1,k}\big|_{XY} = \left(\delta_s - \varphi_{jk}\right)\big|_{XY}$ which implies

$$\delta_s - \varphi_{(j-1)(j-1)}\big|_{XY} = \left[\left(m_s/n_{sym}\right) - \left(n+j-1\right)\right]\psi_{\min};$$

$$\varphi_{jj}\big|_{XY} = \left(n+j-1\right)\psi_{\min}; \text{ and } \delta_s - \varphi_{\left(\frac{m_s}{2}\right)\left(\frac{m_s}{2}\right)}\Big|_{XY} = \left[n + \frac{m_s}{n_{sym}} - 1\right]\psi_{\min}$$

To maximize the Z-spin starting torque, $u_{sj}(t=0) = (-1)^j u_\phi$

$$\frac{T_Z(t=0)}{n_{sym}} = u_\phi \sum_{j=1}^{\left(m_s/n_{sym}\right)+1} c_{jZ} \tag{26}$$

IV. Illustrative Example

Fig. 4(f) illustrates a design example [14] along with its torque function in Fig. 6. Both the rotor and stator have two layers of pole-pairs; eight PMpp's and ten EMpp's respectively. Fig. 4(f) is the plan view (or the projection on the XY-plane) showing the initial locations of the PM's and illustrates the following properties of structural symmetry:

1) Push-pull planes: The stator has five (equally spaced) push-pull planes formed by the 20 EM's. The rotor has four planes formed by 16 PM's.
2) Symmetry about XZ plane: The S2, S3, S4, and S5 EM's are the mirror images of S10, S9, S8 and S7 respectively.
3) Symmetry about YZ plane: The S4, S5, S6, S7 and S8 EM's are symmetrical to the S3, S2, S1, S10, and S9 EM's respectively.
4) When $u_{\phi j+5} = u_{\phi j}$, $u_{\phi j}$ will result in generating a torque about the Z-axis only.

m_r=8,
m_s=10
δ_r=45°,
δ_s=36°
γ_r=20°,
γ_s = 26°
ψ_{min} =9°,
$n_{\max} = 4$
ψ_{sym} =180°,
$n_{sym} = 4$

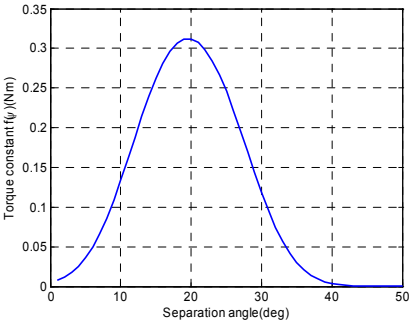

(a) Design (b) torque function as a function of separation angle

Fig. 6 Design parameters and torque function

A. Staring torque for Spin about the Z axis

As an illustration, all the current inputs are assigned a unit magnitude. For a positive starting torque,

$$\frac{T_Z}{2} = c_{1Z}(9°) + \sum_{j=2}^{5} c_{jZ}\left[(45° - j9°), (j9°)\right] + c_{5Z}(45°)$$

where the last term $c_{5Z}(45°) = 0$. ,

$$\Delta T_Z = 4\left[c_{1z}(9°) + c_{2z}(18°) + c_{3z}(27°)\right] \text{ and } T_{Z+} = T_{Z-} = 0$$

Note that if the starting current is maintained, this starting torque will decrease to zero at $\phi = 27°$ and therefore the current pattern must change before reaching $\phi = 3\psi_{\min} = 27°$ in order to maintain the spin rate as shown below:

$$\Delta T_Z\left(\phi = 18°\right) = 2\left[c_{1z}(18°) + 2c_{2z}(27°)\right] \text{ and}$$

$$T_{Z+} = -T_{Z-} = c_{1z}(18°) + 2c_{3z}(9°)$$

$$\Delta T_Z(\phi = 27°) = 0 \text{ and}$$

$$T_{Z+} = -T_{Z-} = 2\left[c_1(27°) + c_{2z}(9°) + c_{5z}(18°)\right]$$

B. Driving Torque for Continuous Spin

For a specified power input, the torque that can be generated depends on the rotor speed. To illustrate this torque-speed relationship, we define the following Speed Number S_N to regulate the spin rate in an open-loop sense:

$$S_N = nj - (n-1) \qquad \text{Where } j = 1, \ldots, m_s/2 \tag{27}$$

The current to regulate the spin-rate takes the form:

$$u_{\phi j} = (-1)^j \,\text{sgn}(\sin\omega_s t)\left|u_m\right| \tag{28}$$

where j = 1, 2, …,5; and $\text{sgn}(x) = 1, -1$ corresponding to $x \ge 0$ and $x < 0$ respectively.

C. Results

Two simulation examples using the torque model are given here. The first illustrates the switching sequences (Table I) as

an electronic gear transmission for 5 speed levels. Due to the geometrical symmetry; only 5 of the 10 stator EMpp's are listed. For example, a controller based on a 9°-step sequence repeats the sequence S_1 to S_{10} in inputting the currents to the EMpp's, while the controller designed for a 45°-step repeats S_1 and S_6= -S_1. The simulated torques for these five speed levels are compared in Fig. 7, where $|u_m|$=1; $2\pi/\omega_s$ = 8ms (corresponding to a sample period limited by Window XP). As shown in Fig. 7, the 9°-step sequence generates much lesser torque ripples but has a low spin rate for a given frequency while the 45°-step sequence is able to generate a high spin rate with the input frequency.

The second simulation estimates the errors due to the torque approximation in (10), where u_ϕ =1A, u_α =0.5A, u_β =0 and Δt =1ms for ϕ =0 to 45° using the 45°-step sequence. Fig. 8 compares the torque computed with and without the approximation; the difference is less than 3.5%.

V. CONCLUSIONS

We present a method of deriving a closed-form torque model for designing the SWM structure and its switching controller. The formulation starts with an approximate 2EM-1PM model and extends to a more general configuration built upon multiple 2EM-1PM torque model. The closed-form torque model given here greatly reduces the torque computation, and simplifies the design of the switching controller. As has been shown, the torque model generally involves $m_s \times m_r$ number of $\mathbf{T}_{jk}$ terms, each of which requires the computation of a time-vary vector cross-product in 3D space. For a SWM with 16 PM's and 20 EM's, this implies 320 computations of $\mathbf{T}_{jk}$ terms. We demonstrate this computational load can be effectively reduced by a two order-of-magnitude (to 8) by the approximate torque in addition to exploiting the structure and symmetry of pole layout of the PM's and EM's. We demonstrate numerically how this torque model can be used to design a switching controller for open-loop speed control that bases on the principle of push-pull operation.

REFERENCES

[1] Clarke, W., 2002, "Mercedes-Benz F-400 Carving," edmunds.com.

[2] Peter, J. 2004 "The Wave of the Future?" Automotive Industries, January.

[3] Lee, K-M. & C.-K. Kwan, 1991, "Design Concept Development of a Spherical Stepper for Robotic Applications," IEEE T-Robotics and Automation, Vol. 7, no.1, pp. 175-180, February 1.

[4] Vachtesevanos, G.J., K. Davey, & K.M. Lee, 1987, "Development of a Novel Intelligent Robotic Manipulator," IEEE Control Systems Magazine, June.

[5] Foggia, A., E. Oliver & F. Chappuis , 1988, "New Three DOF Electromagnetic Actuator," Conference Record – IAS Annual Meeting, Vol. 35, New York.

[6] Hollis, R.L., A.P. Allan, & S. Salcudean, 1987, "A Six Degree-of-freedom Magnetically Levitated Variable Compliance Fine Motion Wrist," Fourth Int'l Symp. on Robotics Research, Santa Cruz.

[7] Kaneko, K., I. Yamada, & K. Itao, 1988, "A Spherical DC Servo Motor with Three Degrees of Freedom," ASM Dyn. Sys. & Con. Div., Vol. 11, p. 433.

[8] Neto, L., R. Mendes, & D. A. Andrade, 1995, "Spherical Motor- a 3D Position Servo," Proc. IEEE Conf. on Electrical Machines and Drives, 11-13 Sept., pp. 227-231.

[9] Lee, K-M., R. Roth, and Z. Zhou, 1996, "Dynamic Modeling and Control of a Ball-joint-like VR Spherical Motor," ASME J. of Dyn. Sys. Meas. and Control, vol. 118, no. 1, pp. 29-40, March.

[10] Chirikjian, G. S., & D. Stein, 1999, "Kinematic Design and Commutation of a Spherical Stepper Motor," IEEE/ASME T-Mechatronics Vol. 4, No. 4, Dec.

[11] Wang, J., G. Jewel, & D Howe, 2003, "Design and Control of a Novel Spherical Permanent Magnet Actuator with Three DOF," IEEE/ASME Trans. on Mechatronics, Vol. 8, No. 4, Dec., 457-467.

[12] Shigeki, T., Osamu, M., & Guoqiang, Z., 1996 "Development of New Generation Spherical Ultrasonic Motor," ICRA96, pp. 2871-2876.

[13] Yang, C. I. & Y. S. Baek, 1999, "Design and Control of the 3 DOF Actuator by Controlling the Electromagnetic Force," IEEE/ASME T-Mechatronics, Vol. 35, No. 5, Sept.

[14] Lee, K.-M. R. A. Sosseh & Z. Wei, 2004, "Effects of the Torque Model on the Control of a VR Spherical Motor," IFAC J. of Contr. Eng. Practice, Vol 12/11 pp 1437-1449.

[15] Lee, K.-M. , H. Son, and J. Joni, **"**Concept Development and Design of a Spherical Wheel Motor (SWM)," *IEEE ICRA* 2005, April 18-22, 2005, Barcelona, Spain.

TABLE I: STATOR EM SWITCHING SEQUENCE (9° INTERVAL)

S_N	EM pole-pair 1	2	3	4	5	N	Switching sequence $S_N = nj-(n-1)$
1	–1	+1	–1	+1	–1	1	$S_N = j$ = 1, 2,..., 10, 1, 2,..., 10,1 2...
2	–1	+1	–1	+1	+1	2	$S_N = 2j-1$ = 1, 3,..., 9,1,3,...,9,1,3...
3	–1	+1	–1	–1	+1	3	$S_N = 3j-2$ = 1, 4,7,1,4,7,1,4...
4	–1	+1	+1	–1	+1	4	$S_N = 4j-3$ = 1, 5, 9, 1, 5, 9, 1, 5,...
5	–1	–1	+1	–1	+1	5	$S_N = 3j-2$ = 1, 6, 1, 6,1,6,1...

TABLE II: SPIN RATE AND AVERAGE TORQUE

Phase angle	9	18	27	36	45
Speed (rpm)	118	236	354	472	590
Torque (Nm)	3.344	3.165	2.485	2.169	1.807

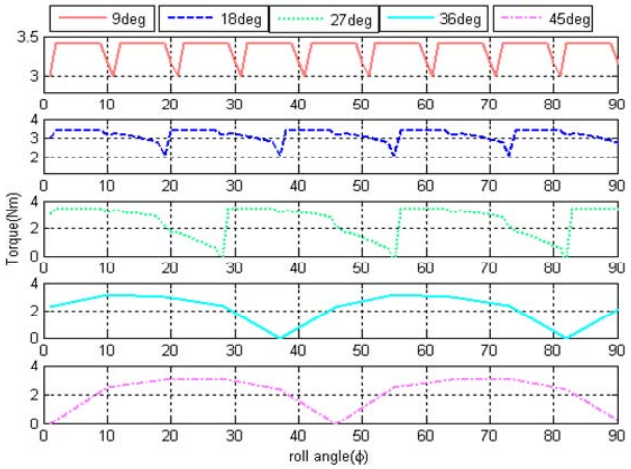

Fig. 7 Torque model for switching sequences

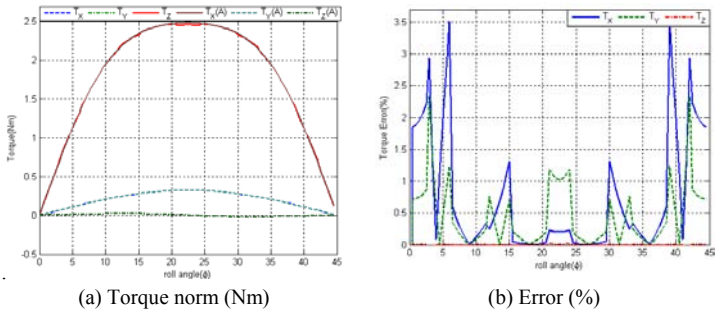

(a) Torque norm (Nm) (b) Error (%)

Fig. 8 Comparison between complete model and approximate model, Equation (10), on computed torque